Diffusion on Nodal and Cylindrical Surfaces

D. Plewczyński, R. Hołyst

Institute of Physical Chemistry PAS and College of Science

Dept. III, Kasprzaka 44/52, 01-224 Warsaw, Poland

9 December 1999

Abstract

We present a catalogue of diffusion coefficients and reorientational angle distributions for various periodic surfaces, such as I-WP, F-RD and S1 nodal surfaces; cylindrical structures like simple, undulated and spiral cylinders, and a three dimensional interconnected-rod structure. The results are obtained on the basis of a simulation algorithm for a diffusion on any surface given by the general equation $\phi(\mathbf{r}) = 0$. They should find applications in the interpretation of the experimental results of the 2D exchange NMR spectroscopy data and optical measurements of the diffusion coefficient of particles embedded in membranes. The mean curvature and a connectivity between parts of surfaces have the main influence on the value of the diffu-

sion coefficient. The surfaces with low mean curvature at every point of the surface are characterized by high diffusion coefficient. However if a surface has globally low mean curvature with large regions of non-zero mean curvature (negative and positive) the effective diffusion coefficient is low, as for example in the case of undulated cylinders. Increasing the connectivity, at fixed curvatures, increases the diffusion coefficient.

PACS numbers: 05.40. +j, 87.64 Hd, 87.22 Bt

1 Introduction

The information about topology of inner membranes in living cells[1,2] can be extracted from transport modes of molecules in biological systems[3,4,5,6,7,8]. In experiments by Shetz *et al.*[6,9,10] small colloidal gold particles perform a random walk in the vicinity of biological membranes. One observes, using a light microscope, a movement of individual gold particles, attached with lectin concanavalin A to a lipid membrane. From its movement one obtains the diffusion coefficient of lipids in the membrane. One also observes the diffusion of proteins embedded in the membranes. Their movement does not show a lipid flow in any direction, so there is no directed transport in biological membranes. There are impenetrable walls on the boundaries of domains in the membrane (for example in the case of erythrocyte). Therefore the free diffusion is observed here only for a limited time. A traveling lipid particle starts to feel the boundaries of the domains in the membrane after 10 seconds[1,9].

Another technique, used by Ghosh and Webb[11], deals with fluorescent lipoproteins (LDL) in a membrane observed by a video microscopy.

The diffusional processes are also observed in amphiphilic systems. The amphiphilic molecules (surfactants) have hydrophobic head and hydrophilic tail. They stabilize various complicated structures in ternary mixtures with water and oil[12,13]. There are many different ordered, bicontinuous phases depending on the temperature and the concentration of surfactant. For low concentrations the amphiphilic molecules form micelles of different shapes,

studied by scattering experiments (light, x-ray, neutrons)[14]. For higher concentration (60% wt) some complex cubic structures are observed in the small angle x-ray scattering experiments[15,16]. These cubic structures are modeled by triply periodic surfaces of constant mean curvature[17], in particular the minimal surfaces (zero mean curvature)[18,19,20]. Using the fluorescent recovery photobleaching technique[15] one computes the diffusion coefficient of particles diffusing along a surface from the measured characteristic times of the recovery curves . The diffusion coefficient is determined with error smaller than 5%.

The effect of lateral diffusion can be investigated by the NMR technique. Here[21] the longitudinal spin relaxation in membranes is sensitive to the internal conformational or rotational motions of individual molecules, with very short correlation times, less than 10^{-8} sec. The transverse spin relaxation time depends on the lateral diffusion, with correlation times greater than 10^{-4} sec. The separation of the time scales shows that the longitudinal spin relaxation is not sensitive to lateral diffusion, while transverse relaxation does depend on diffusion. There are in fact three different mechanisms, which can affect the transverse spin relaxation i.e. lead to the change of the direction of the molecular director axis measured in these experiments: (a) lateral diffusion of molecules on the surface of the membrane, (b) thermally excited undulations of the surface, and (c) the collective director fluctuations. It has been shown by Dolainsky *et al.*[22] that the first mechanism dominates and can alone explain experimental results of the NMR spectroscopy of phospholipids on lipid membranes. A molecule diffusing on the curved membrane

changes its orientation (the long axis of the phospholipid molecule), with respect to the axis fixed in space. However, it keeps the same orientation in the local frame specified by the vector normal to the surface $\mathbf{n}(\mathbf{r})$ during its motion. Therefore $\mathbf{n}(\mathbf{r})$ specifies unambiguously the orientation of a molecule at point $\mathbf{r}$. The change of orientation can be measured experimentally using two dimensional exchange spectroscopy in ^{2}H NMR. It gives the probability $P(\beta, t)$, that after time t the orientation $\mathbf{n}$ changes by the angle β[22,23,24,25]. This probability distribution $P(\beta, t)$ is called the reorientational angle distribution (RAD), which is the space-time correlation function of the orientations of vectors normal to the surface.

Various experimental methods used to investigate diffusional processes on the two dimensional surfaces still suffer from the lack of general theoretical tools to describe more precisely the phenomena of diffusion on any two dimensional mathematical surface. One can find a number of mathematical methods for studying isotropic transport processes on Riemannian manifolds[26,27,28], but they are very complicated and unpractical. Anderson and Wennerström[29] have established an important result concerning the special class of surfaces - the minimal periodic surfaces of cubic symmetry. Such surfaces have zero mean curvature at each point of the surface. Anderson and Wennerström have proved that the effective diffusion coefficient D_{eff} for any minimal surface of cubic symmetry is exactly D_0 (a local surface diffusion constant, like for a plane). However the experimental value $D_{eff}/D_0 \approx 1$ cannot be interpreted as an evidence of the minimal surface, because this relation is valid approximately for any surface of low mean curvatures.

In this paper we study the diffusion on surfaces given by the general equation:

$$\phi(\mathbf{r}) = 0. \tag{1}$$

We try to establish the link between the geometrical and topological properties of the surface and the transport processes on the surface. The topology and shape of the mathematical surface are given by the mean and the Gaussian curvatures, and the Euler characteristic[30]. Here we analyze the random walk of a probe point particle on a mathematical, two dimensional curved surface given by the Eq.1. In our simulations we determine the RAD distribution and the diffusion coefficient for a large class of surfaces.

The paper is organized as follows. In Sec. 2 we present the simulation algorithm. Sec. 3 contains our results for triply periodic, nodal surfaces: I-WP, F-RD and S1[31], and their comparison with the results for other nodal surfaces (P, D and G). In Sec. 4 we describe the influence of the topological decomposition of the S1 surface on diffusion, and the results for the diffusion on some quasi-cylindrical structures. A summary is contained in Sec. 5.

2 The Algorithm for Diffusion on a Curved Surface

The Brownian motion on a two dimensional flat surface is the Wiener-Lévy process[32], which is described by the density distributions:

$$P_1(\mathbf{y}_2, t_2) = \int P_{1|1}(\mathbf{y}_2 - \mathbf{y}_1 | t_2 - t_1) P_1(\mathbf{y}_1, t_1) d\mathbf{y}_1,$$

$$P_{1|1}(\mathbf{y}_2 - \mathbf{y}_1|t_2 - t_1) = \frac{1}{\sqrt{2\pi(t_2 - t_1)}} \exp(-\frac{(\mathbf{y}_2 - \mathbf{y}_1)^2}{2(t_2 - t_1)}),$$

with the initial condition $P_1(\mathbf{y}_1, 0) = \delta(\mathbf{y}_1)$. This process, as a Markov one, satisfies the Chapman-Kolmogorov equation:

$$P_{1|1}(\mathbf{y}_3 - \mathbf{y}_1|t_3 - t_1) = \int P_{1|1}(\mathbf{y}_3 - \mathbf{y}_2|t_3 - t_2) P_{1|1}(\mathbf{y}_2 - \mathbf{y}_1|t_2 - t_1) d\mathbf{y}_2. \quad (2)$$

The process can be discretized in time by introducing the Gaussian operator T_{τ_0} of the elementary, discrete step of duration τ_0. T_{τ_0} is the elementary jump operator with the Gaussian form:

$$T_{\tau_0}(\mathbf{y}_2 - \mathbf{y}_1) = P_{1|1}(\mathbf{y}_2 - \mathbf{y}_1|t_2 - t_1),$$

for $\tau_0 = t_2 - t_1$, and adding rule:

$$T^2_{\tau_0}(\mathbf{y}_3 - \mathbf{y}_1) = \int T_{\tau_0}(\mathbf{y}_3 - \mathbf{y}_2) T_{\tau_0}(\mathbf{y}_2 - \mathbf{y}_1) d\mathbf{y}_2,$$

or using the operator notation:

$$T^2_{\tau_0} = T_{\tau_0} T_{\tau_0} = T_{\tau_0 + \tau_0}.$$

After time t the operator takes the form:

$$T_{t=n\tau_0} = \underbrace{T_{\tau_0} T_{\tau_0} \ldots .}_{\text{n times}} = T^n_{\tau_0}. \quad (3)$$

The equation of the evolution can be rewritten in the form:

$$P(\mathbf{y}, t = n\tau_0) = \underbrace{T_{\tau_0} T_{\tau_0} \ldots .}_{\text{n times}} P(\mathbf{y}, 0) = T^n_{\tau_0} P(\mathbf{y}, 0), \quad (4)$$

where $P(\mathbf{y}, 0) = \delta(\mathbf{y})$ is the initial probability distribution, $P(\mathbf{y}, t)$ is the final distribution, which gives the probability of finding a particle after time t at point $\mathbf{y}$ on the flat surface.

This general method can be used for a curved surface in the following way. At each point of the surface described by the Eq. 1 we define the plane tangent to the surface. At point $\mathbf{r}_0 = (x_0, y_0, z_0)$ the plane is described by the following equation:

$$\mathbf{n}(\mathbf{r}_0)(\mathbf{r} - \mathbf{r}_0) = 0, \tag{5}$$

where $\mathbf{n}(\mathbf{r}_0)$ is the vector normal to the surface. For a convenience we introduce in the tangent plane the local polar coordinates given by the pair of variables: $\{J, \phi\}$. The two dimensional Gaussian operator can be divided onto two operators: the angle rotation operator $T^a_{\tau_0}$ (to choose the direction of the movement - in the ϕ coordinate), and radial jump described by the $T^J_{\tau_0}$, with a proper distribution of jump length J. The resulting operator takes the form:

$$T_{\tau_0}(J, \phi) = T^J_{\tau_0}(J) T^a_{\tau_0}(\phi).$$

Our numerical method[33] consists of a sequence of elementary steps described by the operator T_{τ_0}. A particle at point $\mathbf{r}_0$ jumps along randomly chosen direction ($T^a_{\tau_0}(\phi) = \frac{1}{2\pi}$ operator) in the plane tangent to the surface. The length of the jump J is drawn from the distribution ($T^J_{\tau_0}$ operator):

$$T^J_{\tau_0}(r) = \frac{J}{2D_0\tau_0} \exp\left(-\frac{J^2}{4D_0\tau_0}\right), \tag{6}$$

where D_0 is the local diffusion coefficient, τ_0 is the duration of the elementary time step. After the jump the particle is at point $\mathbf{r}_1$ on the tangent plane ($\mathbf{n}(\mathbf{r}_0)(\mathbf{r}_1 - \mathbf{r}_0) = 0$). Then we project the point $\mathbf{r}_1$ back to the curved surface along the direction given by $\nabla\phi(\mathbf{r}_1)$ (approximately normal to the surface).

The final location is given by the formula:

$$\mathbf{r}_2 = \mathbf{r}_1 - \frac{\phi(\mathbf{r}_1)\nabla\phi(\mathbf{r}_1)}{|\nabla\phi(\mathbf{r}_1)|^2}. \tag{7}$$

The elementary step is next repeated at the point $\mathbf{r}_2$. This algorithm satisfies the detailed balance condition[33].

The mathematical condition necessary for this algorithm to work at all length scales is the continuity of $\phi(\mathbf{r})$, and its first derivatives at each point of the surface[26,30]. This procedure is numerically well defined also for fields with discontinuous first derivatives, if this discontinuity is small enough (see Sec. 4). In our algorithm, which probe a surface with a finite accuracy, one cannot see any roughness of the surface less then a typical jump length.

In our numerical simulations we determine the diffusion coefficient and reorientational angle distribution (RAD). For each surface we compute its mean curvature. The diffusion coefficient is defined here as follows:

$$D_{eff}(t) = \frac{<\mathbf{R}(t)^2>}{4t}, \tag{8}$$

where t is the time of measurement, and

$$\mathbf{R}^2(t) = |\mathbf{r}(t) - \mathbf{r}(0)|^2,$$

is the mean square displacement (in three dimensions) after time t ($\mathbf{r}(0)$ describes the initial position of a random walker in three dimensional space, $\mathbf{r}(t)$ - the final position). The $< ... >$ average is taken with the probability distribution $\varrho(\mathbf{R}, t)$ of finding a particle at time t at point $\mathbf{r}(t)$.

In order to calculate $P(\beta, t)$ we determine first $\cos(\beta(t))$:

$$\cos(\beta(t)) = \mathbf{n}(t) * \mathbf{n}(0), \tag{9}$$

where $\mathbf{n}(t)$ and $\mathbf{n}(0)$ are the normalized vectors normal to the surface in the final and initial position of the walker. Then we transform this distribution to the standard RAD form (distribution of β angle - difference in orientation of two vectors normal to the surface at a starting point, and the final point after time t).

All two dimensional surfaces are characterized here by the modulus of the mean curvature $|H|$, averaged over the whole surface. It is computed using the divergence of the normalized gradient of a field $\phi(\mathbf{r})$, from the following equation[30,34,35] :

$$|H| =< |H(\mathbf{r})| >=< |(-\frac{1}{2}\nabla \cdot \mathbf{n}(\mathbf{r}))| >, \tag{10}$$

where

$$\mathbf{n}(\mathbf{r}) = \frac{\nabla\phi(\mathbf{r})}{|\nabla\phi(\mathbf{r})|}$$

is the unit vector normal to the surface at the point $\mathbf{r}$. The average $< ... >$ is taken over the surface.

To calculate all these quantities in our algorithm we use one random walker, and take the averages over all its trajectories on the surface. Since in the long time limit, this single walker will visit all the points on the surface many times, the precise location of the starting point in the case of connected surfaces is unimportant (ergodicity and Markov nature of the random walk[33]). A typical simulation consists of $K = 3 * 10^3$ runs, each of $M = 10^6$ steps. A typical size of the elementary jump is equal to $L = \sqrt{4D_0\tau_0}$ in comparison to a typical linear size of the unit cell $d \approx 100L$. All averages at time $t = N\tau_0$ are taken over $m = (M - N) * K$ (for $D_{eff}(t)/D_0$ and

$< \cos\beta(t) >$), or $m = M * K$ points (for $< |H| >$), as follows from the formulas:

$$< \cos\beta(t) >= \sum_{j=1}^{K} \sum_{i=1}^{M-N} \frac{\mathbf{n}_j(t_i + t) \cdot \mathbf{n}_j(t_i)}{K * (M - N)}, \tag{11}$$

$$D_{eff}(t)/D_0 = \sum_{j=1}^{K} \sum_{i=1}^{M-N} \frac{|\mathbf{r}_j(t_i + t) - \mathbf{r}_j(t_i)|^2}{K * (M - N)} \frac{1}{D_0} \frac{1}{4t}, \tag{12}$$

and

$$< |H| >= \sum_{j=1}^{K} \sum_{i=1}^{M} (-\frac{1}{2} \nabla \cdot \mathbf{n}(\mathbf{r}_{i,j})). \tag{13}$$

We use each point on a single long trajectory (described by i index) and each run (j index).

The algorithm satisfies the detailed balance condition and is stable[33], providing that steps are smaller than the typical radius of curvature R_1 of the surface. In order to choose the proper jump length L, for the simulation, one must first determine the Gaussian curvature K from the formula[30]:

$$K(\mathbf{r}) = \frac{1}{2}(-(\partial_i n_j)^2 + (\nabla \cdot \mathbf{n}(\mathbf{r}))^2), \tag{14}$$

and $R_1 \approx < \frac{1}{\sqrt{|K(\mathbf{r})|}} >$. In order to compare the time evolution of RAD and D_{eff} for various surfaces, one needs to rescale the size of the unit cell, to have the same surface area per unit cell for all surfaces. The stationary value of D_{eff}, and the stationary limit of RAD's is reached after time proportional to the surface area of a periodic surface inside a unit cell[33].

3 Diffusion on the I-WP, F-RD and S1 Surfaces

The various minimal surfaces have different space symmetries. Each surface of a given symmetry has its analytical representation in terms of infinite Fourier series. If one uses only few terms in this expansion one gets the equation describing the nodal approximation of the minimal surface. The resulting surface is given by the equation in the form of Eq. 1 and has the same space group symmetry as the parent minimal surface. In this section we present the results for the I-WP, F-RD and S1 surfaces. I-WP nodal surface is given by the equation[36] :

$$\begin{aligned} 2(\cos X \cos Y + \cos Y \cos Z + \cos Z \cos X) \\ -(\cos 2X + \cos 2Y + \cos 2Z) = 0, \end{aligned} \tag{15}$$

F-RD nodal surface by[36] :

$$\begin{aligned} -(\cos X \cos Y + \cos Y \cos Z + \cos Z \cos X) + \\ 4 \cos X \cos Y \cos Z = 0, \end{aligned} \tag{16}$$

and S1 nodal surface by[37]:

$$\begin{aligned} \cos X \sin Y \sin 2Z + \cos Y \sin Z \sin 2X + \\ \cos Z \sin X \sin 2Y + 2A_2(cos2X \cos 2Y + \\ \cos 2Y \cos 2Z + \cos 2Z \cos 2X) = 0, \end{aligned} \tag{17}$$

where $X = 2\pi x/d$, $Y = 2\pi y/d$, $Z = 2\pi z/d$, d is the size of the unit cell, and A_2 is a parameter.

In order to compare the results for these surfaces we take different sizes of the unit cells for different surfaces in the units of the jump length $L = \sqrt{4D_0\tau_0}$: $d_{F-RD} = 70L$, $d_{I-WP} = 80L$, and $d_{S1,A_2=0.1} = 60L$, to ensure the same surface area per unit cell for all structures. The RAD's together with the unit cells of the corresponding surfaces are shown on Figs. 1 - 3. In the stationary limit ($lim_{t\to\infty}P(\beta,t)$), two surfaces (I-WP and S1) have almost the same distributions of vectors normal to the surface, similar to the P, D and G nodal surfaces[29,33]. The stationary limits of the time evolution of RADs are similar for almost all known minimal surfaces[20,29,33] and nodal surfaces. The F-RD nodal surface has a very atypical RAD. Its distribution of the vectors normal to the surface has the features of the cubic box (the largest peak for $\beta = \frac{\pi}{2}$, two smaller peaks for $\beta = 0$ and π with approximate proportions of heights $12 : 3 : 3$). In our simulations the time evolution of RAD for the S1 surface is the fastest, the second one is for the F-RD nodal surface, and then successively for I-WP, D, G and P nodal surfaces. It follows that for the fixed area in the unit cell the evolution is faster for surfaces of more complex topology. The topology of the structure is given by its genus g, an integer number which tells us how many holes are in a closed surface. For example the genus for a sphere is zero, while for a torus is one. According to the well known relation: $\chi = 2(1-g)$, the Euler characteristic, χ, is a unambiguously related to the genus g [20,36]. In our case of an infinite periodic surface we compute the Euler characteristic per unit cell. The Euler characteristic for P nodal surface is equal to -4, for D nodal surface $\chi = -16$, and for the G nodal surface $\chi = -8$. Another two surfaces: the nodal I-WP

and the nodal F-RD surface have successively χ equal to -12 and -40. For the nodal S1 surface with $A_2 < 0.5$ we have $\chi = -48$.

The minimal surfaces (for example P, D or G) have the diffusion coefficient D_{eff} equal to D_0[20,29]. Also for the nodal P, D and G surfaces we find the relation $D_{eff} \approx D_0$, since this kind of nodal surfaces closely resemble the minimal surfaces[33]. Different results are obtained for I-WP, F-RD and S1 nodal surfaces. For the F-RD nodal surface $D_{eff} = 0.78D_0$, for nodal I-WP $D_{eff} = 0.96D_0$, and for S1 nodal surface with $A_2 = 0.1$ we have $D_{eff} = 0.98D_0$. The value of D_{eff} is lower than D_0, because these structures have non-zero mean curvatures.

We investigate surfaces with different topology and mean curvatures, but the same symmetry (S1 surfaces for various values of A_2 - see Fig. 4), and the same topology, but different sizes of the unit cell, and therefore rescaled curvatures (F-RD nodal surface for various d). In the first case (the S1 nodal surface) the diffusion coefficient is higher for a lower mean curvature with differences up to 13%. In the second case there is almost no change of the diffusion coefficient. Any deviation of the effective diffusion coefficient from the value D_0 is the sign of the non-zero mean curvatures.

4 Diffusion in Cylindrical Systems

We observe an interesting phenomenon of a topological decomposition of the S1 surface from a complex shape (with Euler characteristic $\chi = -48$) to a quasi-cylindrical structure (zero Euler characteristic: $\chi = 0$) - see Figs. 3

and 5. For $A_2 < 0$ Eq. 17 describes two G nodal surfaces in the unit cell, for $0 < A_2 < 0.5$ we have standard S1 surface (see the bottom picture on Fig. 3), and for $A_2 > 0.5$ we have seven disconnected quasi-cylinders in the unit cell (see the bottom picture on Fig. 5). When we change the value of A_2, we observe a different value and time dependence of the diffusion coefficient (see Fig. 4), and distributions of RADs (see Figs. 3 and 5), because of the changes of the mean curvatures and topology. There is a dramatic decrease of the diffusion coefficient (see Fig. 4) during the transition to another topology (from nodal S1-like to cylindrical). The mean curvature increase 2-4 times in the quasi-cylindrical structure in comparison to the S1 surface.

We have applied the algorithm to study the diffusion on various cylindrical structures. First we take a simple cylinder with the sinusoidal perturbation (see Fig 6):

$$x^2 + y^2 - (R_1 + R_2 \sin[Z])^2 = 0, \tag{18}$$

where $Z = 2\pi z/d$, $R_1 = 33L$, and $R_2 = 10L$. As d varies the mean curvature of the structure changes. Another structure of interest is a spiral DNA-like cylinder (see bottom picture on Fig. 7), described by the equation[38] :

$$\begin{aligned} &\frac{1}{4}x(x+\sqrt{3}y)(-x+\sqrt{3}y)\cos(0.5Z) - \\ &\frac{1}{4}y(\sqrt{3}x+y)(-\sqrt{3}x+y)\sin(0.5Z) - \\ &\qquad \cos(0.5Z) + \frac{1}{500}\exp(x^2+y^2) = 0. \end{aligned} \tag{19}$$

The last cylindrical structure studied here is the three dimensional network

of cylinders (see Fig. 6) described by the equation:

$$\exp(-\frac{x^2}{2d^2\sigma^2}) + \exp(-\frac{y^2}{2d^2\sigma^2}) + \exp(-\frac{z^2}{2d^2\sigma^2}) - 3/2 = 0, \tag{20}$$

for $-\frac{d}{2} \leq x, y, z \leq \frac{d}{2}$. The values of parameters describing the surface are varied as follows: $\sigma = 2$ (thin structure) up to 4.5 (thick structure), and d successively from 113 up to 157. This whole structure is defined as a cubic box with edges of length equal to d repeated over the whole three dimensional space. It has a discontinuity of the first derivatives on the borders of the unit cell equal to $\Delta\partial_{\{x,y,z\}}\phi|_{\{x,y,z\}=\pm d/2} \approx 10^{-3}$. The discontinuity is so small that does not influence our results.

The diffusion coefficient can be used as a measure of the dimensionality of the system (the largest value for 3 dimensional network of cylinders, the lowest for 1 dimensional sinusoidal cylinder), if we keep the mean curvature of the structure constant. On the other hand, in the case of two structures with the same dimensionality, but different mean curvatures, we have much higher diffusion coefficient for thick cylinders (see three dimensional network) i.e. for smaller mean curvature. So instead of changing dimensionality of the system, one can change typical curvatures, with the same effect on the diffusion coefficient: lower mean curvatures means higher diffusion coefficient. The exception from this rule is a sinusoidal cylinder. In that case the lower mean curvature is for strongly undulating structure in comparison to a simple cylinder. The sinusoidal perturbation lowers the diffusion coefficient, because of the longer distance travelled by the random walker along sinusoidal cylinder than along a cylinder. It is due to the distribution of curvatures along the

surface since on the sinusoidal cylinder the regions with lower mean curvature are well separated by the regions with higher mean curvature.

We obtain also interesting results for the diffusion on a DNA-like spiral structure (see Fig. 7). The effective diffusion coefficient for this surface is much smaller ($0.11D_0$) than for a simple straight cylinder ($0.5D_0$), and quite close to the result for the diffusion on a strongly undulating cylinder ($0.1D_0$).

5 Summary

The shape of RAD in the stationary limit can be used as the fingerprint of a structure. Spherical structures (like nodal P, D, G, I-WP, S1 for $A_2 < 0.5$) have sinusoidal RAD:

$$P(\beta) \approx \sin(\beta),$$

cube-like structures (F-RD nodal surface) have 3 peaks in RAD:

$$P(\beta) \approx 3.0 * \delta(\beta) + 12.0 * \delta(\beta - \frac{\pi}{2}) + 3.0 * \delta(\beta - \pi),$$

cylindrical undulated structures have $P(\beta)$ as a constant function, with a sinusoidal term from the perturbation:

$$P(\beta) \approx \frac{1}{\pi} + \sin(\beta),$$

and flat structures (plane, toroidal hole between two flat planes) have strongly peaked distribution of vectors normal to the surface:

$$P(\beta) \approx \delta(\beta) + \delta(\beta - \pi).$$

Using a stationary limit of RAD one can distinguish roughly between spherical, cube-like, cylindrical or flat surfaces.

The diffusion coefficient is a very complex function of the geometry of a structure. Any non-zero mean curvatures changes D_{eff} in comparison to the local diffusion coefficient D_0. If D_0 is the effective diffusion coefficient for a two dimensional plane, then for a free diffusion in a three dimensional volume we have $D_{eff} = \frac{3}{2}D_0$, and for diffusion along a cylinder we have $D_{eff} = \frac{1}{2}D_0$. Using the diffusion coefficient one can distinguish between closed ($D_{eff} = 0$) and open surfaces ($D_{eff} > 0$). For the diffusion along the interconnected cylinders forming a three dimensional network we have $D_{eff} \geq 0.5D_0$, with thick ($D_{eff} \to D_0$) or thin ($D_{eff} \to 0.5D_0$) cylinders. One dimensional undulating or spiral cylindrical structures are characterized by $D_{eff} \leq 0.5D_0$.

In our simulations we observe that changing the mean curvature without changing the topology of the surface, changes the diffusion coefficient by 10-20% (calculated for I-WP, F-RD and S1 nodal surfaces) in comparison to its value for the minimal surfaces. Rescaling the unit cell (simulated for F-RD nodal surface) changes the diffusion coefficient only by 3%. If we change the parameter A_2 in the equation of S1 nodal surface, we observe the change of the structure from the nodal triply periodic surface to the cylindrical surfaces. In this case we observe a dramatic decrease of the diffusion coefficient of the order of 50%.

In the case of cylindrical systems with sinusoidal undulations of a simple cylinder we observe large changes of the diffusion coefficient. This kind of

perturbation lowers the mean curvature (because we sum over regions of negative and positive mean curvatures). But also this type of perturbation lowers the diffusion coefficient, because a walker always has to cross the high mean curvature regions.

If a cylindrical system is more complicated (a three dimensional network of simple cylinders, as in the interconnected-rod model[39]) D_{eff} is larger by 30% than for a simple cylinder. This difference depends on the thickness of the cylinders: for the larger radius of cylinders (smaller mean curvature), we find larger values of the diffusion coefficient for this structure. The connectivity in this case depends on the mean radius of the cylinders connecting the unit cells.

Another result has been obtained for the DNA-like spiral cylinder, where the diffusion coefficient was found to be much smaller ($\sim 80\%$), than in the case of a simple, straight cylinder.

If the investigated surface has regions of large positive or negative mean curvatures one can expect the lower value of the diffusion coefficient. To go from one point to another one must cross regions of large modulus of the mean curvature. This is observed in the case of the sinusoidal perturbated cylinder, and the DNA-like spiral cylinder. The nodal or minimal surfaces have no macroscopic regions of the large, non-zero mean curvature. In this case decreasing the mean curvature increases the diffusion coefficient.

We must yet stress, that the details of the time dependence and stationary values of the measured quantities are very complicated (as one can see on Fig. 9). It is therefore very difficult to describe more precisely the exact

relation between the curvature of a surface and the diffusion coefficient, or the RAD distribution. We hope that this paper will be useful for the experimentalists, who use NMR analysis of RADs or optical measurements of the diffusion coefficient to analyze the relations between geometry and topology of surfaces and the surface diffusion.

6 Acknowledgements

This work was supported by the KBN grant No 2P0B12516. We would like to thank A. Aksimentiev and K. Burdzy for many helpful discussions.

References

[1] D. Haft, M. Edidin, Nature **340**, 262 (1989).

[2] edited by R. Lipowsky, E. Sackmann, *Structure and Dynamics of Membranes, Handbook of Biological Physics,* (Elsevier, Amsterdam, 1995), Vol. I.

[3] K. Berland, P. So, E. Gratton, Biophys. J. **68**, 694 (1995).

[4] R.Swaminathan, C. Hoang, A. Verkman, Biophys. J. **72**, 1900 (1997).

[5] H. Ogawa, S. Inouye, F. Tsuji, K. Yasuda and K. Umesono, Proc. Natl. Acad. Sci. **92**, 11899 (1995).

[6] M. Sheetz, S. Turney, H. Qian and E. Elson, Nature **340**, 284 (1989); G. Lee, A. Ishihara and K. Jacobson, Proc. Natl. Acad. Sci. **88**, 6274 (1991).

[7] P. Mitra, P. Sen, L. Schwartz and P. Le Doussal, Phys. Rev. Lett. **68**, 3555 (1992).

[8] T. Landh, FEBS Letters **369**, 13 (1995).

[9] J. Gelles, B. Schnapp, M. Sheetz, Nature **331**, 450 (1988).

[10] D. Kucik, E. Elson, M. Sheetz, Nature **340**, 315 (1989).

[11] R. Ghosh, W. Webb, Biophys. J. **55**, 498a (1989).

[12] edited by W. Gelbart, A. Ben-Shaul, D. Roux, *Micelles, Membranes, Microemulsions, and Monolayers,* (Springer, New York, 1994).

[13] edited by C. Domb, J. Lebowitz *Self-assembling Amphiphilic Systems, Phase Transitions and Critical Phenomena,* (Academic Press, London, 1994), Vol. 16.

[14] D. Gazeau, S. Hyde, J. Phys. II (France) **5**, 171 (1995).

[15] A. Maldonado, W. Urbach, R. Ober, D. Langevin, Phys. Rev. E **54**, 1774 (1996).

[16] V. Luzzati *et al.* J. Mol. Biol. **229**, 540 (1993).

[17] Z. Wang, S. Safran, Europhys. Lett. **11**, 425 (1990).

[18] S. Hyde *et al.*, *The Language of Shape* (Elsevier, Amsterdam, 1997)

[19] G. Gompper, M. Schick, Phys. Rev. Lett. **65**, 1116 (1990).

[20] W.Góźdź and R.Hołyst, J. Chem. Phys. **106** , 9305 (1997).

[21] C. Dolainsky, A. Möps, T. Bayerl, J. Chem. Phys. **98**, 1712 (1999).

[22] C. Dolainsky, M. Unger, M. Bloom and T. Bayerl, Phys. Rev. E **51**, 4743 (1995).

[23] F. Macquaire and M. Bloom, Phys. Rev. E **51**, 4735 (1995).

[24] C. Dolainsky, P. Karakatsanis and T. Bayerl, Phys. Rev. E **55**, 4512 (1997).

[25] A. Nevzorov, T. Trouard and M. Brown, Phys. Rev. E **55**, 3276 (1997).

[26] N. Ikeda and S. Watanabe, *Stochastic Differential Equations and Diffusion Processes*, (North Holland, Amsterdam), Chapter V, (1981).

[27] M. Pinsky, Trans. AMS **218**, 353 (1976).

[28] Y. Amit Stoch. Process Appl. **37**, 213 (1991).

[29] D. Anderson and H.Wennerström, J. Phys. Chem. **94**, 8683 (1990).

[30] M. Spivak, *A Comprehensive Introduction to Differential Geometry,* (Publish or Perish, Berkeley, 1979), Vol. III.

[31] A.L. Mackay, Proc. R. Soc. Lond. A **442**, 47 (1993).

[32] N.G. van Kampen, *Stochastic processes in physics and chemistry*, (North-Holland, Amsterdam, 1981).

[33] R. Hołyst, D. Plewczyński, A. Aksimientiev, K. Burdzy, Phys. Rev. E **60**, 302 (1999).

[34] I. Barnes, S. Hyde, B. Ninham, J. de Physique Colloque **51 C7**, 19 (1990).

[35] A. Mackay, J. Klinowski, Comp. and Maths. with Appls. **12B**, 803 (1986).

[36] U. Schwartz, G. Gomper, Phys. Rev. E **59**, 5528 (1999).

[37] A. Aksimentiev, R. Ho lyst, J. Chem. Phys. **111**, 2329 (1999).

[38] Michael Jacob, J. Phys. II France, **7**, 1035-1044 (1997).

[39] V. Luzzati, A. Tardieu, T. Gulik-Krzywicki, E. Rivas, F. Reiss-Husson, Nature **220**, 485 (1968).

7 Figure Captions

- Fig. 1 The RAD (top) for the nodal F-RD surface given by Eq. 16 for $t = 64\tau_0$ (circles), $256\tau_0$ (triangles), and $4096\tau_0$ (squares) with the unit cell (bottom) for $d = 70L$. τ_0 is the typical time scale for the duration of the single jump, and L is the typical jump length. The asymptotic long-time diffusion coefficient D_{eff} for this structure is equal to $0.78D_0$. Please note the cube-like distribution of the vectors normal to the surface (a limit of RAD for long times), completely different from the rest of the analyzed nodal structures.

- Fig. 2 The RAD for I-WP nodal structure given by Eq. 15 (the unit cell on the bottom picture), with the size of the unit cell $d = 80L$ for times: $64\tau_0$ (circles), $256\tau_0$ (triangles), and $4096\tau_0$ (squares). For this structure we have $D_{eff} = 0.96D_0$.

- Fig 3 The RAD (top) for the S1 nodal structure given by Eq. 17 (the bottom picture, $d = 60L$), with $A_2 = 0.1$ for $t = 64\tau_0$ (circles), $t = 256\tau_0$ (triangles), and $t = 4096\tau_0$ (squares). This structure is most complicated, and has the diffusion coefficient equal to $0.98D_0$.

- Fig. 4 The diffusion coefficient, as a function of the modulus of the mean curvature $< |H| >$ multiplied by the mean principal radius R_1 of the studied structure. Circles are for the S1 nodal surface (Fig 3), squares are for cylindrical surfaces (Fig. 5). One can see a dramatic change of the mean curvature $< |H| >$ (75%), and the diffusion coefficient D_{eff}

(50%). The Euler characteristic changes from -48 for S1 (Fig 3) to 0 for cylinders (Fig 5) with no symmetry change of the structure.

- Fig. 5 The RAD (top) for a disconnected quasi-S1 structure given by Eq. 17 with $A_2 = 0.8$, and $d = 162L$ for the same times as on Figs. 1, 2, 3. This structure consists of seven undulating cylinders (see the bottom picture) and has $D_{eff} = 0.46D_0$, which is very close to the diffusion coefficient for a sinusoidally perturbated cylinder (see Fig. 6).

- Fig. 6 The RAD (top) of the sinusoidally perturbated cylinder (bottom) given by Eq. 18 with $d = 44L$, with $D_{eff} = 0.1D_0$ (see also the legend of Fig. 1).

- Fig. 7 The RAD (top) of the spiral DNA-like cylinder (bottom) given by Eq. 20 for times: $64\tau_0$ (circles), $256\tau_0$ (triangles), and $4096\tau_0$ (squares), and $d = 70L$, with $D_{eff} = 0.11D_0$. The same diffusion coefficient is observed for sinusoidally undulated cylinder with $d = 44L$ (see Fig. 6).

- Fig. 8 The RAD for a three dimensional network of thin cylinders given by Eq. 20 (top) with $d = 115L$, for times $64\tau_0$ (circles), $256\tau_0$ (triangles) and $4096\tau_0$ (squares). The unit cell of this structure is shown on the bottom picture. For $\sigma = 2.0$ in Eq. 20 we have $D_{eff} = 0.61D_0$.

- Fig. 9 The diffusion coefficient D_{eff}/D_0 for all investigated, open structures as a function of the area-averaged modulus of the mean curvature $< |H| >$ multiplied by the mean principal radius R_1 of the curvature for the surface. Circle $\bigcirc$ represent result[33] for P, D, G nodal surfaces.

Square $\square$ is for the S1 surface with $A_2 = 0.1$, star $\bigstar$ for F-RD nodal surface and the plus sign $+$ for I-WP nodal surface. For cylindrical systems we have: $\Diamond$ for various three dimensional networks of cylinders, $\triangleleft$ for a simple cylinder (with R_1 equal to the radius of the cylinder), $\triangle$ for sinusoidal undulated cylinders, and $\bigtriangledown$ for a DNA-like spiral structure.

8 Figures

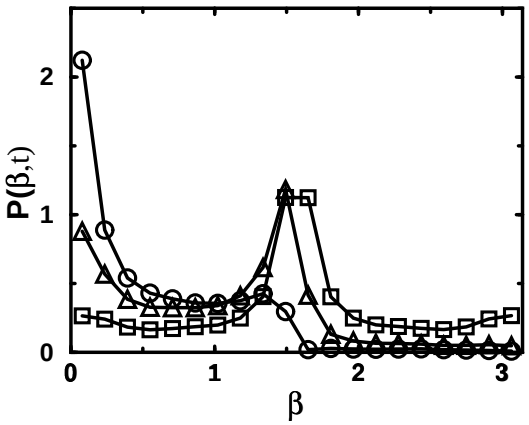

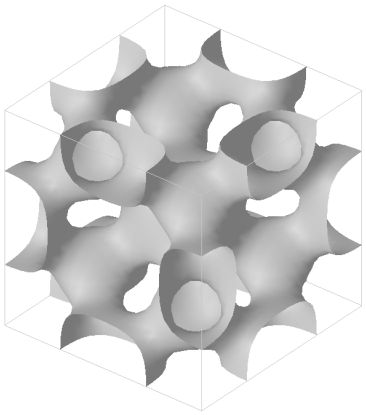

Figure 1.

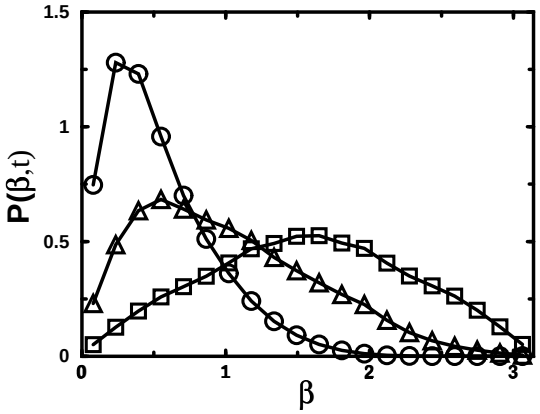

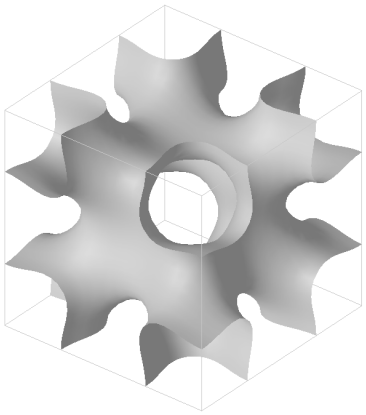

Figure 2.

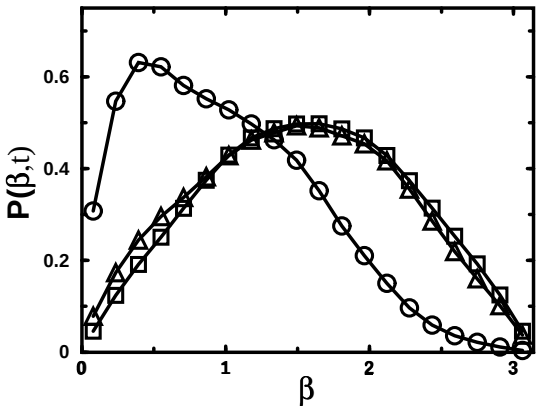

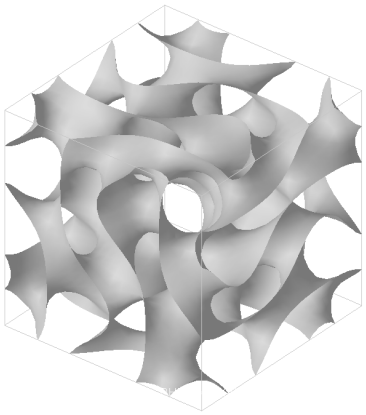

Figure 3.

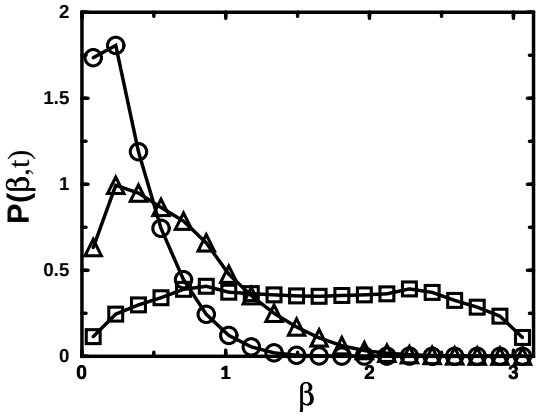

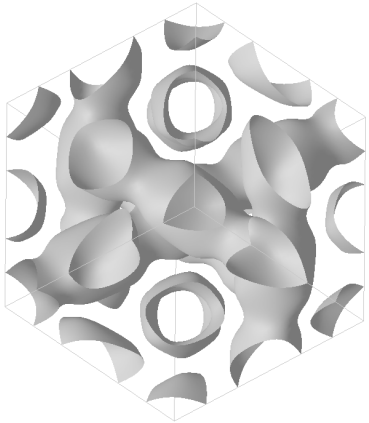

Figure 5.

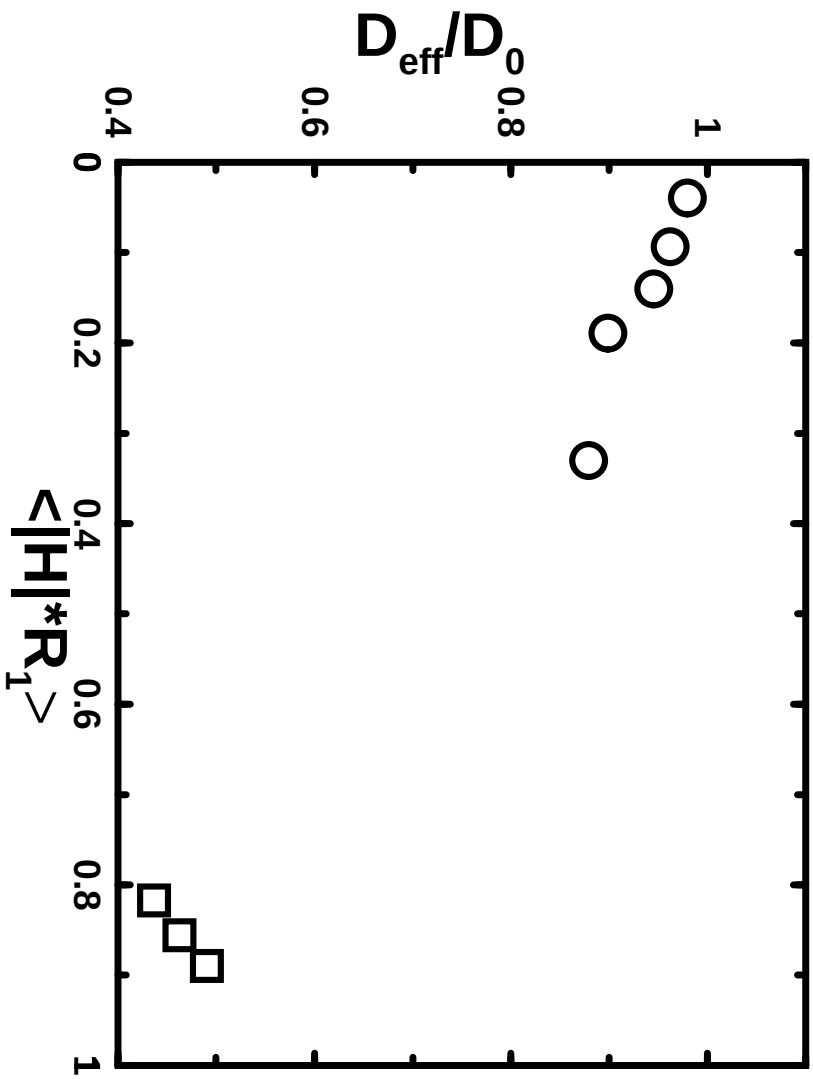

Figure 4.

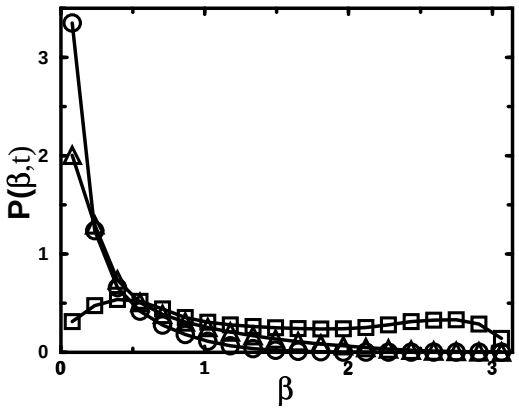

Figure 7.

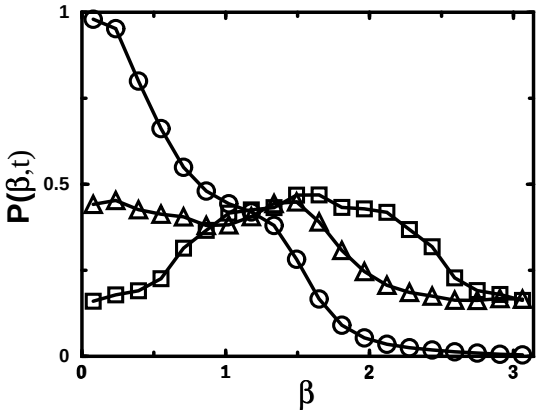

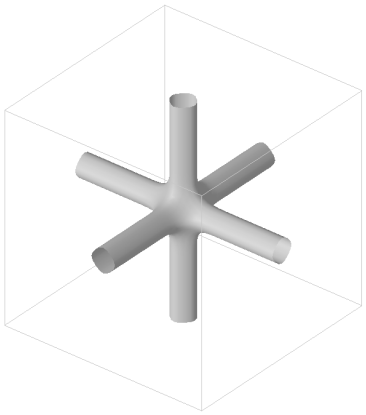

Figure 8.

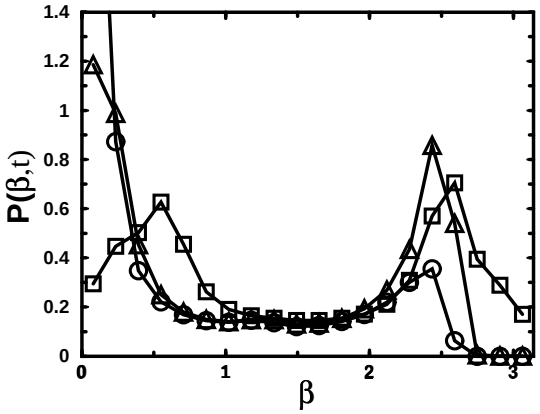

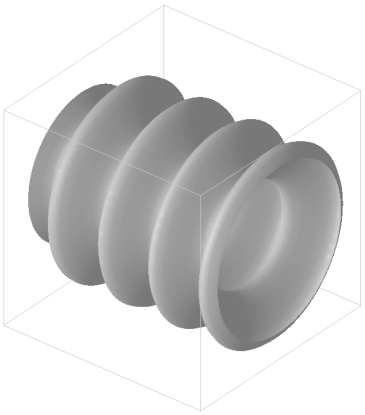

Figure 6.

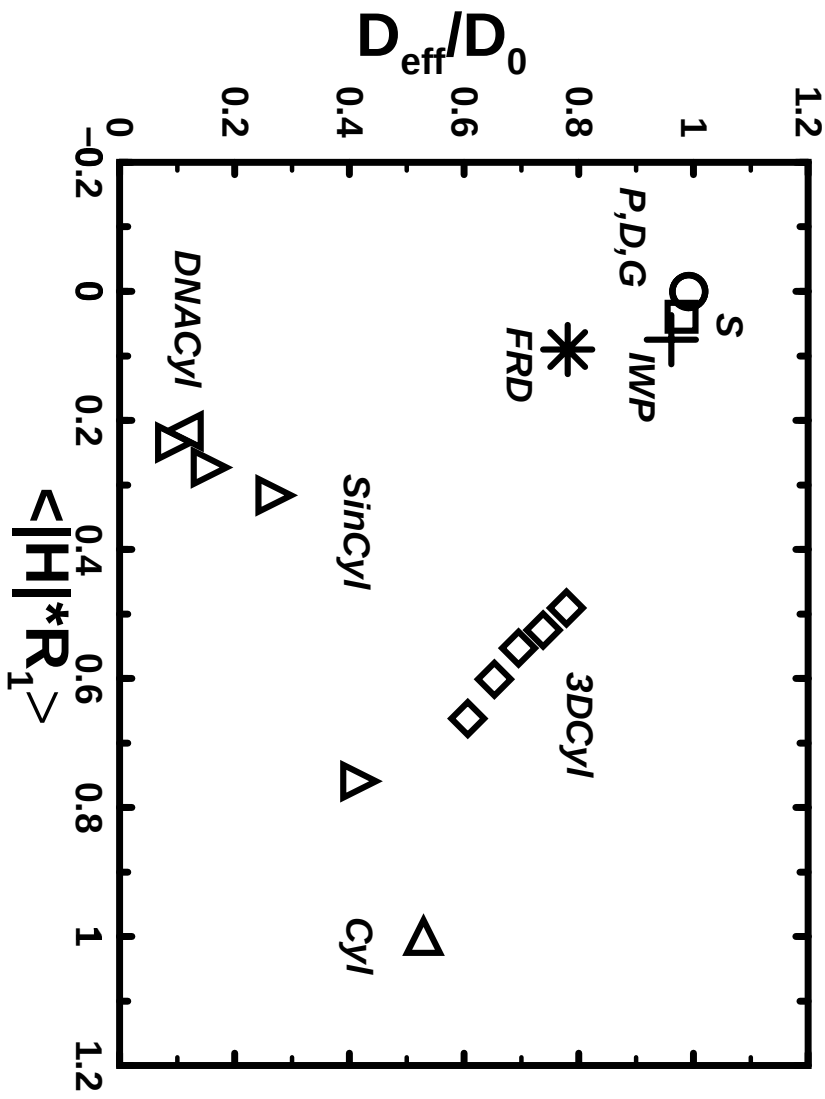
D_{eff}/D_0
1.2
1
0.8
0.6
0.4
0.2
0
−0.2
0
0.2
0.4
0.6
0.8
1
1.2
$\langle|H|*R_1\rangle$
S
IWP
P,D,G
FRD
3DCyl
SinCyl
Cyl
DNACyl

Figure 9.